Joint Transmit Waveform and Receive Filter Design for Dual-Function Radar-Communication Systems

Christos G. Tsinos [ID], *Senior Member, IEEE*, Aakash Arora [ID], *Student Member, IEEE*,
Symeon Chatzinotas [ID], *Senior Member, IEEE*, and Björn Ottersten [ID], *Fellow, IEEE*

Abstract—In this paper, the problem of joint transmit waveform and receive filter design for dual-function radar-communication (DFRC) systems is studied. The considered system model involves a multiple antenna base station (BS) of a cellular system serving multiple single antenna users on the downlink. Furthermore, the BS simultaneously introduces sensing capabilities in the form of point-like target detection from the reflected return signals in a signal-dependent interference environment. A novel framework based on constrained optimization problems is proposed for the joint design of the transmit waveform and the radar receive filter such that different constraints related to the power amplifiers and the radar waveform are satisfied. In contrast to the existing approaches in the DFRC systems' literature, the proposed approach does not require the knowledge of a predetermined radar beampattern in order to optimize the performance of the radar part through its approximation. Instead, a beampattern is generated by maximizing the radar receive signal-to-interference ratio (SINR) thus, enabling a more flexible design. Moreover, the radar receive filter processing and its optimization is considered for the first time on DFRC systems, enabling the effective exploitation of the available degrees of freedom in the radar receive array. Efficient algorithmic solutions with guaranteed convergence are developed for the defined constrained nonconvex optimization problems. The effectiveness of the proposed solutions is verified via numerical results.

Index Terms—Radar-communication, beamforming, precoding, waveform design, MIMO, spectrum sharing, multiuser interference, nonconvex optimization, alternating optimization, gradient-projection (GP).

I. INTRODUCTION

THE rise of the 5th Generation (5G) and beyond wireless technologies brings huge demands for high quality wireless communications services, since numerous different devices are expected to be interconnected. By 2022, 28.5 billion interconnected devices [1] are expected, spanning from regular cellular networks to small-scale smart devices under the concept of the so-called "Internet of Things (IoT)" [2], [3].

Thus, additional frequency spectrum resources are more than necessary to wireless communication systems in order to meet those demands. To that end, a promising solution is the efficient utilization of the electromagnetic spectrum, currently occupied by other applications. Among the different propositions [4]- [6], the case of joint communications-radar spectrum sharing has recently concentrated great interest in the literature [7]–[9]. The latter is usually implemented via two different approaches: 1) Coexistence of the radar and the communication systems and 2) Dual-function radar-communication (DFRC) system design.

In the first one, the design of the transmit signals from the two systems is done independently while managing the cross interference to each other in order to avoid a possible degradation on their performance [10]–[15]. Therefore, cooperation between the two systems is required in real-time that perplexes the system design and results in increased complexity and communication overhead.

The second one, aims at the design of systems that can jointly handle the operations of the radar and the communication systems. Such a design may apply in real-time the joint sensing/communication operations via a single hardware setup. To that end, the DFRC system is implemented via designing the transmit waveform such that both radar/communication-related performance metrics are optimized and spatial/temporal constraints are satisfied, respectively. This approach appropriately exploits the available spatial degrees of freedom in the DFRC system, i.e., multiple transmit antennas. For this multiple input-multiple output (MIMO) system, the designed transmit waveform enables the transmission at high information rates to the intended users while maintaining a reliable operation for the radar system.

In [16], the transmit waveform is directly designed by minimizing the multiuser interference (MUI) such that a desired radar beampattern is achieved by imposing constraints on the covariance matrix of the transmit signals. In [17], linear precoding solutions are derived such that the designed signals to be transmitted match the desired radar beampattern, guarantee the required signal-to-interference ratio (SINR) level at the intended users and satisfy a transmission power constraint. A similar approach with improved performance was followed in [18] where the precoding matrix is decomposed into two parts, one for the communication and the other for the radar system. A different

view is presented in [19]. There, a vehicular DFRC system is proposed that transmits a single waveform and extracts both radar and communication parameters at the intended receiver through efficient processing.

In the existing literature on the DFRC systems [16]–[18], the waveform designs are derived such that only transmission energy/power related constraints are mainly satisfied. On the other hand, the radar waveform usually has to satisfy additional spatial/temporal constraints, e.g., constant-modulus [20], [21], similarity to a known waveform [22], [23], etc. Furthermore, the existing works on the DFRC systems aim to optimize the performance of the radar part by minimizing the distance to/imposing a predetermined beampattern in the designed radar waveform. On the contrary, in the MIMO radar-only literature, there are several works that optimize the radar performance without the need of a predetermined beampattern [24]–[29]. In those cases, the radar transmission waveform is designed by maximizing the radar receive signal-to-interference ratio (SINR). Since the detection probability of a target is an monotonically increasing function of the radar output SINR [26], the radar performance can be optimized without the knowledge of a predetermined beampattern, leading to a more flexible design. Moreover, the existing works on the DFRC systems do not consider the application/design of a radar receive filter in their system model. In literature so far, the application/design of radar receive filters has been solely considered for radar-only systems [24]–[29]. To that end, the aim of the present work is to propose a novel framework for the joint design of the transmit waveform and the radar receive filter of a DFRC system based on the MUI minimization/radar receive SINR maximization criteria. The proposed framework is able to design transmit waveforms that simultaneously satisfy both communications and radar specific spatial/temporal constraints.

The contributions of the present work are summarized as follows.

- A novel design for a DFRC system with radar receive filtering is proposed.
- The transmit waveform and the radar receive filter of the DFRC system are jointly designed such that both the MUI in the communications system and the receive SINR at the radar's side are optimized. The SINR maximization criterion for optimizing the performance of the radar part is considered for the first time in the literature of DFRC systems.
- The transmit waveform is designed while satisfying different spatial/temporal constraints for the first time in the literature. The cases of 1) total transmission energy, 2) constant-modulus, 3) total transmission energy-plus-similarity and 4) constant-modulus-plus-similarity constraints are considered.
- In order to jointly design the transmit waveform and the radar receive filter subject to the aforementioned spatial/temporal constraints, four different nonconvex constrained optimization problems are formulated. This is the first time that these problems are studied in the open literature and as a consequence, they have no known solutions. To that end, we develop novel algorithmic solutions based on the alternating optimization and gradient-projection

(GP) frameworks that have fast convergence to a stationary point. Furthermore, we establish the convergence of the proposed solutions to a Karush-Kuhn-Tucker (KKT)-point of the respective problems.

- Numerical results verify the excellent performance of the proposed solutions under different simulation setups. We also compare the performance of the proposed algorithms to known benchmarks that independently optimize the transmit signals of the communication and the radar systems.

The rest of the paper is organized as follows. Section II describes the considered system model for the DFRC system. In Section III, the optimization problems for the joint transmit waveform and radar receive filter design are formulated for the different cases of the considered spatial/temporal constraints. Section IV derives the algorithmic solutions to the previously defined optimization problems. Section V presents the numerical results and Section VI concludes this work.

Notation. Upper-case and lower-case bold letters are used to define matrix and vector variables, respectively. The $N \times N$ identity matrix is denoted by $\mathbf{I}_N$. The $N \times 1$ vector of zeros is denoted by $\mathbf{0}_N$. $\mathbb{C}$ and $\mathbb{R}$ are the complex and the real numbers' domains, respectively. $|\cdot|$ denotes the modulus of a complex number. $\nabla_{\mathbf{x}}$ denotes the gradient with respect to the variable $\mathbf{x}$. $\mathbb{E}\{\cdot\}$ is the expectation operator. $\|\cdot\|_2$, $\|\cdot\|_\infty$, and $\|\cdot\|_F$ denote the l_2, l_∞ and Frobenius norms, respectively. $(\cdot)^H$ and $(\cdot)^T$ denote the Hermitian and the transpose of a vector/matrix, respectively. $\text{vec}(\cdot)$ is the vectorization operator. $\mathbf{A} \otimes \mathbf{B}$ is the Kronecker product of matrices $\mathbf{A}$ and $\mathbf{B}$. $\text{Re}\{\cdot\}$ is the real part of the complex operand.

II. SYSTEM MODEL

Let us consider a narrow-band DFRC system equipped with an uniform linear array (ULA) of T elements with half-wavelength inter-element spacing. The DFRC system serves M single antenna user terminals (UTs) on the downlink operation and simultaneously transmits radar probing waveforms for point-like target detection. Let us further assume that the DFRC system is also equipped with a dedicated ULA of R elements for receiving the radar signals, following the model of a radar system with collocated transmit and receive antenna arrays [24]–[29]. The system model is shown in Fig. 1. In Subsections II-A and II-B, the operation of the communication and the radar part are described in detail. Then, in Subsection II-C, the operation protocol of the DFRC system is presented.

A. Communication Model

By dropping the time index for simplicity, the received signals at the communication UTs in N symbol times are given by,

$$\mathbf{Y} = \mathbf{H}\mathbf{X} + \mathbf{Z}, \tag{1}$$

where $\mathbf{Y} \in \mathbb{C}^{M \times N}$ is a matrix whose entry $y_{m,n}$ is the signal received at the mth UT on the nth symbol time, $1 \le m \le M$, $1 \le n \le N$, $\mathbf{X} = [\mathbf{x}_1, \ldots, \mathbf{x}_N] \in \mathcal{X}$ is the $T \times N$ transmit signal matrix for the N symbol times, $\mathcal{X}$ is a set of spatial/temporal constraints on the transmitted signals which are discussed in
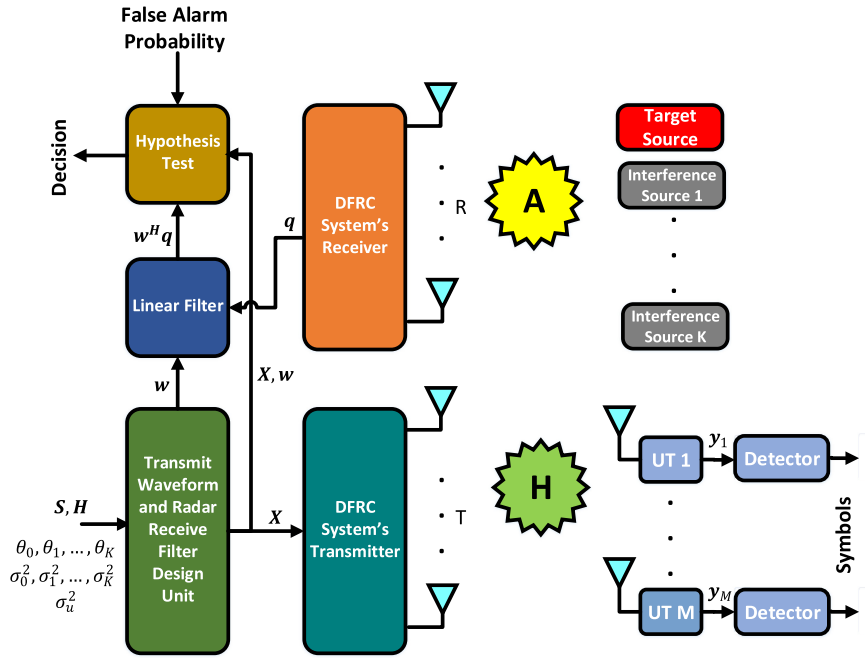
Fig. 1.   DFRC system model.

Section III, $\mathbf{x}_n$ denotes the transmit vector from the DFRC system's antennas at symbol time n, $\mathbf{H} = [\mathbf{h}_1, \ldots, \mathbf{h}_M]^T \in \mathbb{C}^{M \times T}$ is the matrix of the frequency-flat fading channels between the DFRC system and the UTs, $\mathbf{h}_m$ is the $T \times 1$ vector of channel coefficients between the DFRC transmitter and the mth UT, modeled as $\mathcal{CN}(0, \mathbf{I}_T)$, $\mathbf{Z} = [\mathbf{z}_1, \ldots, \mathbf{z}_N]$ is the Additive White Gaussian Noise (AWGN) matrix variable that corrupts the corresponding transmissions, $\mathbf{z}_n \sim \mathcal{CN}(0, \sigma_z^2 \mathbf{I}_M)$ and σ_z^2 denotes the noise variance.

The communication part of the system aims at the transmission of a desired symbol $s(m, n) \in \mathcal{O}$, $1 \leq m \leq M$, $1 \leq n \leq N$, from the DFRC system to the mth UT in the nth symbol time. $\mathcal{O}$ is the set of the employed constellation points. In each symbol time, the vector of the symbols to be transmitted to the UTs is denoted by $\mathbf{s}_n \in \mathcal{O}^{M \times 1}$. Given the CSI and $\mathbf{s}_n$, the communication part of the DFRC system aims at the design of a transmit signal vector, $\mathbf{x}_n$, such that the received vector signal $\mathbf{y}_n$ is as close to $\mathbf{s}_n$, as possible.

The latter may be achieved by minimizing the so-called "MUI energy" [16], [30], given by,

$$f(\mathbf{X}) = \|\mathbf{H}\mathbf{X} - \mathbf{S}\|_F^2, \tag{2}$$

where $\mathbf{S} = [\mathbf{s}_1, \ldots, \mathbf{s}_N]$ is the matrix of the stacked symbols over the N symbol times. Observe that the received signal of the mth UT in the nth symbol time can be written as,

$$y_{m,n} = s_{m,n} + \underbrace{\mathbf{h}_m^T \mathbf{x}_n - s_{m,n}}_{\text{MUI at the } m\text{th user}} + z_{m,n}. \tag{3}$$

Then, according to (3), the receive SINR per block of N symbols for the mth user is defined as

$$\xi_m = \frac{\mathbb{E}\{|s_{m,n}|^2\}}{\mathbb{E}\{|\mathbf{h}_m^T \mathbf{x}_n - s_{m,n}|^2\} + N_0}, \tag{4}$$

where $s_{m,n}$ is the (m, n)th entry of the symbol matrix $\mathbf{S}$. The expectation operator in the numerator is applied on $s_{m,n}$ and in the denominator is applied on $s_{m,n}$ and $\mathbf{x}_n$, as well.

It has been shown in [30] that the achievable information rate for the mth user is a function of ξ_m in (4). Thus, the achievable sum-rate of the communication part can be expressed as,

$$r = \sum_{m=1}^{M} \log_2(1 + \xi_m). \tag{5}$$

Let us assume that 1) the symbols $s_{m,n}$, $1 \leq m \leq M$, $1 \leq n \leq N$ are drawn from the same constellation set $\mathcal{O}$ and have fixed energy and 2) the channel matrix $\mathbf{H}$ is perfectly estimated at the DFRC system, e.g. via a training-based method [31]. Then, the signal power $\mathbb{E}\{|s_{m,n}|^2\}$ in (4) is also fixed and thus, the SINR expression per user can be maximized by minimizing the MUI energy in (2). From (5), it is straightforward to see that by maximizing the SINR of the UTs, their achievable rate is maximized, as well. That is, the MUI energy (2) minimization is a suitable criterion for optimizing the performance of the communication system.

Note that the signals to be transmitted are designed in a block basis, i.e., for N symbol times (matrix $\mathbf{X}$). Furthermore, observe that the optimal transmit signals that convey the desired symbols to the intended UTs are directly designed through the minimization of the least-squares function in (2). That is, the transmit signal matrix $\mathbf{X}$ is derived in a nonlinear manner without the need of a linear precoder.

B. Radar Model

We may now move to the description of the radar model. For the transmitted $T \times 1$ signal $\mathbf{x}_n$, $1 \leq n \leq N$ by the antennas of the DFRC system, the signal seen at a location with angle θ is

given by,

$$\mathbf{a}_t^T(\theta)\mathbf{x}_n, \;\; n = 1, \ldots, N, \tag{6}$$

where $\mathbf{a}_t(\theta)$ denotes the $T \times 1$ transmit steering vector. As discussed in the beginning of the present section, here, we assume that a ULA with half-wavelength inter-element spacing is employed and thus, the steering vector is given by,

$$\mathbf{a}_t(\theta) = \frac{1}{\sqrt{T}}\left[1, e^{-j\pi\sin(\theta)}, \ldots, e^{-j\pi(T-1)\sin(\theta)}\right]^T. \tag{7}$$

Let us assume that the target is located at angle θ_0 and that there are also K signal-dependent interference sources located at angles $\theta_k \neq \theta_0$, $k = 1, \ldots, K$. We further assume that any possible self-interference between the transmit and the radar receive array is mitigated by employing an appropriate method [32]. The baseband vector of signals at the radar receive array in the nth symbol time is given by,

$$\mathbf{q}_n = \alpha_0 \mathbf{a}_r(\theta_0)\mathbf{a}_t^T(\theta_0)\mathbf{x}_n$$
$$+ \sum_{k=1}^{K} \alpha_k \mathbf{a}_r(\theta_k)\mathbf{a}_t^T(\theta_k)\mathbf{x}_n + \mathbf{u}_n, \tag{8}$$

where α_0 and α_k are the complex amplitudes of the target and the kth interference source with $\mathbb{E}\{|\alpha_0|^2\} = \sigma_0^2$, and $\mathbb{E}\{|\alpha_k|^2\} = \sigma_k^2$, respectively, $\mathbf{u}_n$ is a circular symmetric complex white Gaussian noise vector with zero mean and covariance matrix equal to $\sigma_u^2\mathbf{I}_R$, σ_u^2 is the noise variance and $\mathbf{a}_r(\theta)$ is the $R \times 1$ vector of the propagation delays from a source located at angle θ to the radar receive elements. Again, under the assumption of a ULA with half-wavelength inter-spacing between adjacent elements, we have that

$$\mathbf{a}_r(\theta) = \frac{1}{\sqrt{R}}\left[1, e^{-j\pi\sin(\theta)}, \ldots, e^{-j\pi(R-1)\sin(\theta)}\right]^T. \tag{9}$$

Note that in the previous, the angle of arrival in the radar receive array is assumed to be the same with the angle of departure of the transmit signal from the DFRC system. This is a reasonable assumption within the relevant literature [24]–[29] given that the transmit and the radar receive array are collocated. Of course in practice, these two angles might differ, due to multi-path phenomena, for example. Nevertheless, if both the actual angles of arrival and departure can be estimated, the proposed methodology is directly applicable for the design of the DFRC system.

By setting $\mathbf{x} = \text{vec}(\mathbf{X})$, $\mathbf{q} = \text{vec}(\mathbf{Q})$ and $\mathbf{u} = \text{vec}(\mathbf{U})$, where $\mathbf{Q} = [\mathbf{q}_1, \ldots, \mathbf{q}_N]$ and $\mathbf{U} = [\mathbf{u}_1, \ldots, \mathbf{u}_N]$, (8) can be rewritten as

$$\mathbf{q} = \alpha_0 \mathbf{A}(\theta_0)\mathbf{x} + \sum_{k=1}^{K} \alpha_k \mathbf{A}(\theta_k)\mathbf{x} + \mathbf{u}, \tag{10}$$

where $\mathbf{A}(\theta)$ is defined for angle θ as

$$\mathbf{A}(\theta) = \mathbf{I}_N \otimes \left[\mathbf{a}_r(\theta)\mathbf{a}_t^T(\theta)\right]. \tag{11}$$

A common approach to design the radar waveform is based on the maximization of the output SINR. This is the case since the detection probability is usually an monotonically increasing function of the output SINR [23], [26]. It is assumed that a linear $RN \times 1$ finite impulse response (FIR) filter $\mathbf{w}$ is applied at the radar receive array for maximizing the output SINR. The filter output is given by,

$$c = \mathbf{w}^H\mathbf{q}$$
$$= \alpha_0 \mathbf{w}^H\mathbf{A}(\theta_0)\mathbf{x} + \mathbf{w}^H \sum_{k=1}^{K} \alpha_k \mathbf{A}(\theta_k)\mathbf{x} + \mathbf{w}^H\mathbf{u}. \tag{12}$$

Then, the output SINR can be expressed as,

$$\gamma(\mathbf{x}, \mathbf{w}) = \frac{\sigma_0^2|\mathbf{w}^H\mathbf{A}(\theta_0)\mathbf{x}|^2}{\mathbf{w}^H\left[\sum_{k=1}^{K}\sigma_k^2\mathbf{A}(\theta_k)\mathbf{x}\mathbf{x}^H\mathbf{A}^H(\theta_k)\right]\mathbf{w} + \sigma_u^2\mathbf{w}^H\mathbf{w}}. \tag{13}$$

Under the assumption that the DFRC system is able to estimate θ_k and σ_k^2 for $k = 0, 1, \ldots K$, the optimal waveform $\mathbf{x}$ and filter $\mathbf{w}$ can be derived via the SINR maximization criterion. This way, we optimize the performance at the radar's side in terms of its target detection probability, as well. This is achieved by designing a transmit waveform and radar receive filter such that deep nulls are placed in specific directions to reject the signals coming from the interfering sources while keeping distortionless response in the target signal's direction. That is, a beampattern is automatically generated that aims at the maximization of the radar receive SINR. Note that the required information regarding the interfering sources may be obtained by using an environmental dynamic database, following a cognitive radar paradigm, as in [33]–[35].

C. Operation Protocol of the DFRC System

This section is closed with the description of the operation protocol of the DFRC system. The operation flow-chart is presented in Fig. 2. As we can see, the DFRC system's operation is divided into four stages. In the first one, the DFRC system estimates the required information related to the communication system's channel matrix and the angles and the complex gains of the target and interference sources, as well. In the second stage, based on the estimated information and the desired symbols to be transmitted to the UTs in the next N symbol times, the DFRC system jointly designs the corresponding transmit signal matrix $\mathbf{X}$ and the radar receive filter $\mathbf{w}$. In the third one, the derived signals in $\mathbf{X}$ are transmitted for N symbol times. Based on the received signals, the UTs are able to directly detect the transmitted symbols. During this period, the DFRC radar receive array, receives also the reflected signals from the target and the interference sources. In the final stage, the transmission of the signals in matrix $\mathbf{X}$ is completed. The filter $\mathbf{w}$ is applied on the radar receive signals and the detection of the target source is examined such that a predetermined false alarm probability is preserved.
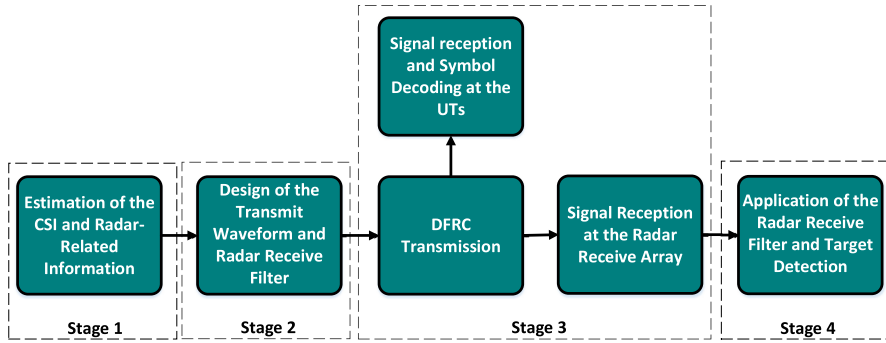
Fig. 2.   Operation flow-chart of the DFRC system.

III. PROBLEM FORMULATION

In this section, we formulate four optimization problems via which the optimal transmit waveform and the radar receive filter are jointly designed. These optimization problems differ in the spatial/temporal constraints that are imposed on the transmit waveform. The cases of total transmission energy (TE), constant-modulus (CM), total transmission energy-plus-similarity (TE+SIM) and constant-modulus-plus-similarity (CM+SIM) constraints are considered. Before proceeding further, let us first focus on how the function of both the communication and the radar part can simultaneously be optimized.

At this point, it is instructive to highlight that the DFRC system optimization requires the knowledge of the channel matrix $\mathbf{H}$ and the radar parameters θ_k and σ_k^2 for $k = 0, 1, \ldots, K$. Note that the estimation methods that are employed by the independent communication and radar systems can be employed by the DFRC system, as well. That is, the channel matrix can be estimated via a training based scheme [31] and the radar parameters can be estimated as discussed in the end of Section II-B.

As discussed in Sections II-A and II-B, the communication part of the DFRC system requires the minimization of the objective function in (2), in order to design the transmit signals in $\mathbf{X}$ such that the desired symbols in $\mathbf{S}$ are conveyed to the intended UTs. Furthermore, the radar part of the DFRC system may maximize the detection probability by maximizing the SINR expression in (13). Clearly, the simultaneous optimization of both of the communication and radar parts is not a straightforward task. Among the different approaches for solving such a multi-objective optimization problem [36], we opt for the weighted sum method that combines the two objective functions into a composite one. Thus, the composite objective function is given by

$$f_c(\mathbf{x}, \mathbf{w}) = \rho f'(\mathbf{x}) + (1 - \rho)\frac{1}{\gamma(\mathbf{x}, \mathbf{w})}, \qquad (14)$$

where $f'(\mathbf{x}) = \|\tilde{\mathbf{H}}\mathbf{x} - \mathbf{s}\|_2^2$, $\tilde{\mathbf{H}} = \mathbf{I}_N \otimes \mathbf{H}$ and $\rho \in \mathbb{R}$ is a parameter that enables the trade-off between the communication and the radar performance.

It is evident from (14) that by selecting the ρ value to be close to 1, a higher weight is imposed on the minimization

of $f'(\mathbf{x})$. Thus, the DFRC system favors the performance of the communications part over the radar one. Contrariwise, as ρ moves towards 0, a higher weight is allocated to the minimization of $1/\gamma(\mathbf{x}, \mathbf{w})$ or equivalently to the the maximization of the SINR expression $\gamma(\mathbf{x}, \mathbf{w})$. Therefore, the DFRC system opts for a better radar performance over the one of the communication part. Thus, a flexible performance trade-off between the radar and the communication objectives is achieved.

We may now proceed to the different problem formulations considering the four different cases of spatial/temporal constraints, discussed above.

A. Total Transmission Energy Constraint

The TE or total transmission power constraint has been extensively employed in the communications' literature to model the limitations of the power amplifiers (PAs) at the transmitter's side [37]. First works on the MIMO radar domain have also considered the SINR maximization problem under a constraint on the total transmission energy [24], [38], [39]. In case of the DFRC system, the optimization problem to be solved under the TE constraint is defined as,

$$(\mathcal{P}_1): \qquad \min_{\mathbf{x}, \mathbf{w}} \rho f'(\mathbf{x}) + (1 - \rho)\frac{1}{\gamma(\mathbf{x}, \mathbf{w})}$$
$$s.t. \ \|\mathbf{x}\|_2^2 \leq P_{max},$$

where P_{max} is the maximum transmission energy, supported by the DFRC system.

B. Constant-Modulus Constraint

The CM constraint is highly desirable in real-world communication as well as radar systems due to its low Peak-to-Average-Ratio (PAR) property. The possible large envelope fluctuations of the transmission signals could lead to significant nonlinear distortions by the transmitter's PAs. In order to avoid the undesirable distortion, each PA has to work in its linear region, resulting in low power efficiency, [40]. On the contrary, CM transmission signals are not affected by the distortions produced by amplitude nonlinearities when appropriate filtering is used, [41]. In this

case, the optimization problem to be solved is defined, as

$$(\mathcal{P}_2): \quad \min_{\mathbf{x},\mathbf{w}} \rho f'(\mathbf{x}) + (1-\rho)\frac{1}{\gamma(\mathbf{x},\mathbf{w})}$$

$$s.t. \ |x_n| = \sqrt{\frac{P_{max}}{TN}}, \ 1 \le n \le TN,$$

where x_n is the nth entry of $\mathbf{x}$ and the modulus $|x_n|$ is set to $\sqrt{P_{max}/(TN)}$ in order to have the same total transmission energy per block of N symbols with the case of $(\mathcal{P}_1)$.

C. Similarity Constraint

While the maximization of the SINR expression in (13) achieves the maximization of the detection probability, as well, it does not necessarily results in a transmit waveform that has good ambiguity properties, i.e., a narrow main peak both in range and in Doppler and relatively low sidelobe peaks. Transmit waveforms with good ambiguity properties are desired in the radar systems since they enable the reliable estimation of the so-called "Doppler frequency". The latter is very important since it is directly related to the target radial velocity which is required for tracking the target and classifying its dangerousness [23], [42].

A common approach followed in the literature is to consider a similarity constraint on the SINR maximization problem. The similarity constraint forces the designed waveform to be close to a reference one in some sense. As a reference waveform is used a known one that possesses the desirable properties. Nevertheless, the addition of the similarity constraint comes at the cost of inferior receive SINR and as a consequence, lower target detection probability. As it is evident, the closer a waveform is to the reference one, the better is the approximation of its desirable properties and the higher is the degradation on the detection performance.

In radar-only studies, the similarity constraint is usually enforced via a constraint on the l_2 or the l_∞ norm of the difference of the designed waveform to the reference one, i.e.,

$$\|\mathbf{x} - \mathbf{x}_0\|_2^2 \ (\|\mathbf{x} - \mathbf{x}_0\|_\infty) \le \epsilon, \tag{15}$$

where $\mathbf{x}_0$ is the reference waveform and $\epsilon \in \mathbb{R}$ is a parameter for controlling the degree of the similarity. In the case of a communication system, such a strict constraint would have severe impact on the performance of the system, as well. Since the similarity constraint is related to the radar system only, a more flexible approach would be to connect this constraint to the trade-off parameter ρ, used to tune the performance between the radar and communication parts of the DFRC system. This can be done by relaxing the similarity constraint and bringing it as a penalty term on the cost function of the optimization problem under consideration. More specifically for the cases of the TE and CM constraints we have,

$$(\mathcal{P}_3): \quad \min_{\mathbf{x},\mathbf{w}} \rho f'(\mathbf{x}) + (1-\rho)\frac{1}{\gamma(\mathbf{x},\mathbf{w})} + (1-\rho)\lambda\|\mathbf{x} - \mathbf{x}_0\|_2^2$$

$$s.t. \ \|\mathbf{x}\|_2^2 \le P_{max},$$

and

$$(\mathcal{P}_4): \quad \min_{\mathbf{x},\mathbf{w}} \rho f'(\mathbf{x}) + (1-\rho)\frac{1}{\gamma(\mathbf{x},\mathbf{w})} + (1-\rho)\lambda\|\mathbf{x} - \mathbf{x}_0\|_2^2$$

$$s.t. \ |x_n| = \sqrt{\frac{P_{max}}{TN}}, \ 1 \le n \le TN,$$

respectively. $\lambda \in \mathbb{R}$ is a penalty parameter. That is, by appropriately tuning the ρ and λ values, we can achieve the desired operation point regarding to the performance of the communication-radar parts and the similarity to a reference waveform, as well.

IV. ALGORITHMIC FRAMEWORK FOR THE JOINT TRANSMIT WAVEFORM-RADAR RECEIVE FILTER DESIGN

In this section, we develop algorithmic solutions to problems $(\mathcal{P}_1) - (\mathcal{P}_4)$. The aforementioned problems are nonconvex due to the involved nonconvex cost function and the nonconvex CM constraint in $(\mathcal{P}_2)$ and $(\mathcal{P}_4)$. Before proceeding towards the algorithmic solutions development, first we observe that all the problems involve a differentiable objective function. Moreover, later in the present section, we show that the orthogonal projection on the constraint sets of problems $(\mathcal{P}_1) - (\mathcal{P}_4)$, can be computed in closed-form. These two facts lead to the development of algorithmic solutions based on the alternating minimization and GP frameworks.

A. Algorithms

Problems $(\mathcal{P}_1)$ and $(\mathcal{P}_2)$ share the same objective function which is differentiable in both $\mathbf{w}$ and $\mathbf{x}$. We refer to this common objective function with the term $g(\mathbf{x},\mathbf{w})$. Also, problems $(\mathcal{P}_3)$ and $(\mathcal{P}_4)$ have the same objective function which has a penalty term to enforce similarity constraints in addition to the objective function of problems $(\mathcal{P}_1) - (\mathcal{P}_2)$. The term $g'(\mathbf{x},\mathbf{w})$ is used to denote that function. Furthermore, $(\mathcal{P}_1)$ and $(\mathcal{P}_3)$ have to satisfy the TE constraint which can be written in set form as, $\mathcal{X}_{TE} = \{\mathbf{x} \in \mathbb{C}^{TN \times 1} | \|\mathbf{x}\|_2^2 \le P_{max}\}$. In a similar manner, $(\mathcal{P}_2)$ and $(\mathcal{P}_4)$ have to satisfy the CM constraint which is expressed in set form as $\mathcal{X}_{CM} = \{\mathbf{x} \in \mathbb{C}^{TN \times 1} | |x_n| = \sqrt{P_{max}/(TN)}, 1 \le n \le TN\}$. As all the problems are nonconvex but have differentiable objective functions with respect to both $\mathbf{w}$ and $\mathbf{x}$, we adopt the alternating minimization framework, as discussed above. The steps of the derived algorithm are given by,

$$\mathbf{x}^{(k+1)} = \arg\min_{\mathbf{x} \in \mathcal{X}_{TE} \text{ or } \mathbf{x} \in \mathcal{X}_{CM}} g(\mathbf{x},\mathbf{w}^{(k)}) \text{ or } g'(\mathbf{x},\mathbf{w}^{(k)})$$

$$(16)$$

$$\mathbf{w}^{(k+1)} = \arg\min_{\mathbf{w}} (1-\rho)\frac{1}{\gamma(\mathbf{x}^{(k+1)},\mathbf{w})}, \tag{17}$$

where $\mathbf{x}^{(k)}$ and $\mathbf{w}^{(k)}$ are the solutions available to problems (16) and (17), respectively, at the k-th iteration. As can be seen from (17), the first term of the original objective functions $g(\mathbf{x},\mathbf{w})$ and $g'(\mathbf{x},\mathbf{w})$ is ignored, as it is independent of $\mathbf{w}$.

Problem (17) can be simplified as,

$$\mathbf{w}^{(k+1)} = \arg\max_{\mathbf{w}} \frac{1}{(1-\rho)}\gamma(\mathbf{x}^{(k+1)},\mathbf{w}). \tag{18}$$

Algorithm 1: Joint Waveform and Filter Design for the DFRC System.

1: Initialize $k = 0$, $\mathbf{w} \in \mathbb{C}^{RN \times 1}$ and $\mathbf{x} \in \mathcal{X}_{TE}$ for $(\mathcal{P}_1)$ and $(\mathcal{P}_3)$ or $\mathbf{x} \in \mathcal{X}_{CM}$ for $(\mathcal{P}_2)$ and $(\mathcal{P}_4)$;

2: **while** not converged **do**

3:    $k \leftarrow k + 1$

4:    Compute the gradient of g for $(\mathcal{P}_1)$ and $(\mathcal{P}_2)$ from (23) or g' for $(\mathcal{P}_3)$ and $(\mathcal{P}_4)$ from (24);

5:    Update $\mathbf{d}^{(k+1)}$ using (21);

6:    Compute $\Pi_{\mathcal{X}_{TE}}\{\mathbf{d}^{(k+1)}\}$ for $(\mathcal{P}_1)$ and $(\mathcal{P}_3)$ from (25) or $\Pi_{\mathcal{X}_{CM}}\{\mathbf{d}^{(k+1)}\}$ for $(\mathcal{P}_2)$ and $(\mathcal{P}_4)$ from (26);

7:    Update $\mathbf{w}^{(k+1)}$ from (20);

8: **end while**

return $\mathbf{x}$, $\mathbf{w}$

Now problem (18) can be further written as,

$$\max_{\mathbf{w}} \frac{1}{(1-\rho)} \mathbf{w}^H \left[\sum_{k=1}^{K} \sigma_k^2 \mathbf{A}(\theta_k) \mathbf{x}^{(k+1)} (\mathbf{x}^{(k+1)})^H \mathbf{A}^H(\theta_k) \right] \mathbf{w}$$
$$+ \sigma_u^2 \mathbf{w}^H \mathbf{w}$$

$$\text{s.t. } \mathbf{w}^H \mathbf{A}(\theta_0) \mathbf{x} = 1. \tag{19}$$

The above problem admits the following closed-form solution,

$$\mathbf{w}^{(k+1)} = \frac{(\mathbf{B}^{(k)})^{-1} \mathbf{A}(\theta_0) \mathbf{x}^{(k+1)}}{(\mathbf{x}^{(k+1)})^H \mathbf{A}^H(\theta_0)(\mathbf{B}^{(k)})^{-1} \mathbf{A}(\theta_0) \mathbf{x}^{(k+1)}}, \tag{20}$$

where $\mathbf{B}^{(k)} = \sum_{k=1}^{K} \sigma_k^2 \mathbf{A}^H(\theta_k) \mathbf{x}^{(k+1)} (\mathbf{x}^{(k+1)})^H \mathbf{A}(\theta_k) + \sigma_u^2 \mathbf{I}$. Now, we focus on solving (16) via the GP framework.

The core of the GP framework [43] is the iterative steps, given by

$$\mathbf{d}^{(k+1)} = \mathbf{x}^{(k)} - \alpha^{(k)} \nabla_{\mathbf{x}} \bar{g}(\mathbf{x}^{(k)}, \mathbf{w}^{(k)}) \tag{21}$$

$$\mathbf{x}^{(k+1)} = \Pi_{\mathcal{X}} \left\{ \mathbf{d}^{(k+1)} \right\}, \tag{22}$$

where $\alpha^{(k)}$ is a suitable step-size parameter in the k-th iteration, $\Pi_{\mathcal{X}}\{\cdot\}$ denotes the orthogonal projection onto set $\mathcal{X}$, $\bar{g}(\mathbf{x}^{(k)}, \mathbf{w}^{(k)})$ can be either $g(\mathbf{x}^{(k)}, \mathbf{w}^{(k)})$ or $g'(\mathbf{x}^{(k)}, \mathbf{w}^{(k)})$ and $\mathcal{X}$ can be either $\mathcal{X}_{TE}$ or $\mathcal{X}_{CM}$ based on the optimization problem under consideration. Furthermore, the gradient vectors for those two cases are given by,

$$\nabla_{\mathbf{x}} g(\mathbf{x}^{(k)}, \mathbf{w}^{(k)}) = 2(1-\rho) \frac{(|b^{(k)}|^2 \mathbf{G}^{(k)} \mathbf{x}^{(k)})}{|b^{(k)}|^4}$$
$$- 2(1-\rho) \frac{(\mathbf{x}^{(k)})^H \mathbf{G}^{(k)} |b^{(k)}|^2}{|b^{(k)}|^4}$$
$$+ 2\rho(-\tilde{\mathbf{H}}^H \mathbf{s} + \tilde{\mathbf{H}}^H \tilde{\mathbf{H}} \mathbf{x}^{(k)}), \tag{23}$$

and

$$\nabla_{\mathbf{x}} g'(\mathbf{x}^{(k)}, \mathbf{w}^{(k)}) = \nabla_{\mathbf{x}} g(\mathbf{x}^{(k)}, \mathbf{w}^{(k)}) + 2(1-\rho)\lambda(\mathbf{x} - \mathbf{x}_0), \tag{24}$$

respectively, where $b^{(k)} = (\mathbf{x}^{(k)})^H \mathbf{A}^H(\theta_0) \mathbf{w}^{(k)}$ and $\mathbf{G}^{(k)} = \sum_{k=1}^{K} \sigma_k^2 \mathbf{A}(\theta_k) \mathbf{w}^{(k)} (\mathbf{w}^{(k)})^H \mathbf{A}^H(\theta_k)$.

Let us now proceed with the derivation of the projection operator $\Pi_{\mathcal{X}_{TE}}\{\cdot\}$. The constraint related to set $\mathcal{X}_{TE}$ may be enforced by solving the following optimization problem,

$$(\mathcal{P}_5): \quad \min_{\mathbf{x}^\dagger} \ \|\mathbf{x}^\dagger - \mathbf{x}\|_2^2$$

$$\text{s.t. } \mathbf{x}^\dagger \in \mathcal{X}_{TE},$$

where $\mathbf{x}^\dagger$ is the projection of $\mathbf{x}$ onto $\mathcal{X}_{TE}$. Problem $(\mathcal{P}_5)$ is convex and from its KKT conditions, it can be shown that

$$\mathbf{x}^\dagger = \begin{cases} \mathbf{x}, & \|\mathbf{x}\|_2^2 \leq P_{max} \\ \sqrt{P_{max}} \frac{\mathbf{x}}{\|\mathbf{x}\|_2}, & \|\mathbf{x}\|_2^2 > P_{max} \end{cases}. \tag{25}$$

The projection operator $\Pi_{\mathcal{X}_{CM}}\{\cdot\}$ may be derived by solving a similar problem to $(\mathcal{P}_5)$, i.e.,

$$(\mathcal{P}_6): \quad \min_{\mathbf{x}^\ddagger} \ \|\mathbf{x}^\ddagger - \mathbf{x}\|_2^2$$

$$\text{s.t. } \mathbf{x}^\ddagger \in \mathcal{X}_{CM},$$

where $\mathbf{x}^\ddagger$ is the projection of $\mathbf{x}$ onto the set $\mathcal{X}_{CM}$. As can be seen, $(\mathcal{P}_6)$ is separable in each one of the elements $x_n^\ddagger$ and x_n, $1 \leq n \leq TN$, of vectors $\mathbf{x}$ and $\mathbf{x}^\ddagger$, respectively. One may show that these decoupled scalar problems admit a closed-form solution given by

$$x_n^\ddagger = \begin{cases} \sqrt{\frac{P_{max}}{TN}}, & \mathbf{x}_n = 0 \\ \sqrt{\frac{P_{max}}{TN}} \frac{x_n}{|x_n|}, & \mathbf{x}_n \neq 0 \end{cases}. \tag{26}$$

The complete algorithm summarizing the steps for solving problems $(\mathcal{P}_1)$-$(\mathcal{P}_4)$ is presented in Algorithm 1.

We close this subsection with a brief discussion on the computational complexity of Algorithm 1. As can be seen, the variable $\mathbf{w}$ is updated at every iteration using a closed-form solution in (20) and the vector $\mathbf{x}$ is updated using a GP step which requires the computation of the objective function's gradient. These two steps involve basic matrix-vector and matrix-matrix, multiplications and additions. The per-iteration complexity of Algorithm 1 is $O(T^3 N^3)$ as the primary operation that dominates the computational complexity is the matrix inversion, $(\mathbf{B}^{(k)})^{-1}$. Note that the complexity of the proposed method is comparable to the one of the state of the art works in MIMO radar literature [24], [26], [29], [38]. As presented in the Introduction, those works develop solutions for the simpler problem of the joint transmit waveform and radar receive filter design in radar only systems. That is, the proposed DFRC system design is able to accommodate the functions of both the radar and the communication systems without significant impact on the required computational overhead.

B. Convergence Analysis

First we note that problems $(\mathcal{P}_1)$-$(\mathcal{P}_4)$ are solved by using the corresponding version of the derived Algorithm 1 which is based on the alternating optimization and GP frameworks. Moreover, all of them have a differentiable objective function. Thus, for simplicity we prove the convergence for problem $(\mathcal{P}_1)$ based on the results in [44] and a similar proof follows for the remaining problems, as well.

Theorem 1: A sequence of iterates generated by Algorithm 1, $\{\mathbf{x}^{(k)}, \mathbf{w}^{(k)}\}$, converges to a KKT-point of problem $(\mathcal{P}_1)$.

Proof: Problem (17) admits a closed-form solution and problem (16) is solved using a GP step. Therefore, first we analyze the solution in (21), (22) of problem (16). It can be seen that the solution in (21), (22) is a minimizer of the following function over the considered constraint set, $\mathcal{X}_{TE}$,

$$\tilde{g}(\mathbf{x}; \mathbf{x}^{(k)}, \mathbf{w}^{(k)}) = g(\mathbf{x}^{(k)}, \mathbf{w}^{(k)})$$
$$+ \mathrm{Re}\left\{\nabla_{\mathbf{x}} g(\mathbf{x}^{(k)}, \mathbf{w}^{(k)})^H (\mathbf{x} - \mathbf{x}^{(k)})\right\}$$
$$+ \frac{1}{2\alpha^{(k)}} \left\|\mathbf{x} - \mathbf{x}^{(k)}\right\|_2^2, \qquad (27)$$

where $\alpha^{(k)} < \frac{1}{L^{(k)}}$ and $L^{(k)}$ is the smallest Lipschitz constant of the function g at the k-th iteration. Now, it can be seen that the function $\tilde{g}$ satisfies the following properties,

$$g(\mathbf{x}, \mathbf{w}^{(k)}) \leq \tilde{g}(\mathbf{x}; \mathbf{x}^{(k)}, \mathbf{w}^{(k)}), \forall \mathbf{x} \qquad (28)$$

$$g(\mathbf{x}^{(k)}, \mathbf{w}^{(k)}) = \tilde{g}(\mathbf{x}^{(k)}; \mathbf{x}^{(k)}, \mathbf{w}^{(k)}) \qquad (29)$$

$$\nabla_{\mathbf{x}} g(\mathbf{x}^{(k)}, \mathbf{w}^{(k)}) = \nabla_{\mathbf{x}} \tilde{g}(\mathbf{x}^{(k)}; \mathbf{x}^{(k)}, \mathbf{w}^{(k)}), \qquad (30)$$

where (28) follows from $\alpha^{(k)} < \frac{1}{L^{(k)}}$. Now considering the updates in (16) and (17), we have the following inequalites,

$$g(\mathbf{x}^{(k)}, \mathbf{w}^{(k)}) = \tilde{g}(\mathbf{x}^{(k)}; \mathbf{x}^{(k)}, \mathbf{w}^{(k)}) \qquad (31)$$

$$\geq \tilde{g}(\mathbf{x}^{(k+1)}; \mathbf{x}^{(k)}, \mathbf{w}^{(k)}) \qquad (32)$$

$$\geq g(\mathbf{x}^{(k+1)}, \mathbf{w}^{(k)}) \qquad (33)$$

$$\geq g(\mathbf{x}^{(k+1)}, \mathbf{w}^{(k+1)}), \qquad (34)$$

where (31) follows from (29), (32) holds because of (16), (33) follows from (28) and (34) is obtained because the problem with respect to $\mathbf{w}$ is solved in closed-form as given by (20).

Let us now consider a convergent subsequence $\{\mathbf{x}^{(k_j)}, \mathbf{w}^{(k_j)}\}$ with a limit point $(\mathbf{x}^{(\infty)}, \mathbf{w}^{(\infty)})$. Based on the minimization steps (16) and (17) we have,

$$\tilde{g}(\mathbf{x}; \mathbf{x}^{(k_j)}, \mathbf{w}^{(k_j)}) \geq \tilde{g}(\mathbf{x}^{(k_j+1)}; \mathbf{x}^{(k_j)}, \mathbf{w}^{(k_j)}) \qquad (35)$$

$$\geq g(\mathbf{x}^{(k_j+1)}, \mathbf{w}^{(k_j)}) \qquad (36)$$

$$\geq g(\mathbf{x}^{(k_j+1)}, \mathbf{w}^{(k_j+1)}) \qquad (37)$$

$$\geq g(\mathbf{x}^{(k_{j+1})}, \mathbf{w}^{(k_{j+1})}) \qquad (38)$$

$$= \tilde{g}(\mathbf{x}^{(k_{j+1})}; \mathbf{x}^{(k_{j+1})}, \mathbf{w}^{(k_{j+1})}), \qquad (39)$$

where (35)–(39) can be shown by following similar arguments to the ones used to prove (31)–(34), in the above. Now, by utilizing the continuity of the function $\tilde{g}$ and taking the limit $j \to \infty$ on both the sides of (39), we obtain,

$$\tilde{g}(\mathbf{x}; \mathbf{x}^{(\infty)}, \mathbf{w}^{(\infty)}) \geq \tilde{g}(\mathbf{x}^{(\infty)}; \mathbf{x}^{(\infty)}, \mathbf{w}^{(\infty)}). \qquad (40)$$

The inequality (40) implies that $\mathbf{x}^{(\infty)}$ is a block-wise minimizer of the function $\tilde{g}(\cdot)$ and satisfies the following partial-KKT condition with respect to $\mathbf{x}$ as given by,

$$\nabla_{\mathbf{x}} \tilde{g}(\mathbf{x}^{(\infty)}; \mathbf{x}^{(\infty)}, \mathbf{w}^{(\infty)}) + 2\mu^{(\infty)} \mathbf{x}^{(\infty)} = \mathbf{0}_{TN}, \qquad (41)$$

where $\mu^{(\infty)} \in \mathbb{R}_+$ denotes the optimal dual solution associated with the TE constraint. Now utilizing (30) in (41), we obtain,

$$\nabla_{\mathbf{x}} g(\mathbf{x}^{(\infty)}, \mathbf{w}^{(\infty)}) + 2\mu^{(\infty)} \mathbf{x}^{(\infty)} = \mathbf{0}_{TN}. \qquad (42)$$

The condition (41) shows that $\mathbf{x}^{(\infty)}$ is a block-wise minimizer of problem (16). On the similar lines, we can show that,

$$g(\mathbf{x}^{(k_j)}, \mathbf{w}) \geq g(\mathbf{x}^{(k_j)}, \mathbf{w}^{(k_j)}) \qquad (43)$$

$$g(\mathbf{x}^{(\infty)}, \mathbf{w}) \geq g(\mathbf{x}^{(\infty)}, \mathbf{w}^{(\infty)}). \qquad (44)$$

The inequality (44) shows that $\mathbf{w}^{(\infty)}$ is a block-wise minimizer of function g and satisfies the following partial KKT-condition,

$$\nabla_{\mathbf{w}} g(\mathbf{x}^{(\infty)}, \mathbf{w}^{(\infty)}) = \mathbf{0}_{RN}. \qquad (45)$$

Combining the partial KKT-conditions (42) and (45), we prove that a solution sequence generated by Algorithm 1 converges to a KKT-point of problem $(\mathcal{P}_1)$.

V. NUMERICAL RESULTS

In this section, numerical results are presented for evaluating the performance of the proposed techniques. A DFRC system with $T = 16$ antennas at the transmitter and $R = 8$ antennas at the radar receiver is considered. The DFRC system serves $M = 4$ UTs while aiming at the detection of a target source at spatial angle $\theta_0 = 15^o$. Furthermore, 3 interfering sources are assumed to be located at spatial angles $\theta_1 = -50^o$, $\theta_2 = -10^o$ and $\theta_3 = 40^o$. The power of target signals is set to $\sigma_0^2 = 10$ dB. The power of the interference signals is set to $\sigma_k^2 = 30$ dB for $k = 1, 2, 3$. The noise variance at the radar receiver is equal to $\sigma_u^2 = 0$ dB. The employed antenna ULAs are considered to have half-wavelength inter-element separation. The symbols to be transmitted to the UTs are drawn uniformly from a Binary Phase Shift Keying (BPSK) modulation. The constellation points are normalized to unit power. The number of symbols per block is set to $N = 20$. The maximum allowed power per block of symbols is set to $P_{max} = 20$ W. The orthogonal linear frequency modulation (LFM) is considered as a reference waveform. The space-time matrix $\mathbf{X}_0$ of the LFM waveform is given by,

$$\mathbf{X}_0(l, n) = \sqrt{\frac{P_{max}}{TN}} e^{2j\pi \frac{(n-1)(l+n-1)}{N}}, \qquad (46)$$

where $l = 1, \ldots, T$, $n = 1, \ldots, N$ and $\mathbf{X}_0(l, n)$ is the (l, n)th entry of $\mathbf{X}_0$. The reference sequence $\mathbf{x}_0 \in \mathbb{C}^{TN \times 1}$ is calculated as $\mathbf{x}_0 = \mathrm{vec}(\mathbf{X}_0)$. Note that LFM waveforms present good pulse compression and ambiguity properties while performing well in distinguishing point targets [45]. On the other hand, they may present poor performance in environments with clutter. Fixed step-size parameters $a^{(k)}$ for all the algorithms are employed such that the optimal performance is attained. The results are averaged over 100 different blocks of symbols and 1000 channel realizations. The channel coefficients are modeled as $\mathcal{CN}(0, 1)$.

A. Benchmarks

Prior proceeding to the presentation of the results, let us provide a brief discussion about the benchmarks used for comparison purposes in the present paper. We start with the benchmark

for the communication part of the DFRC system. This involves the design of the transmit signals such that the MUI function in (2) is minimized subject to the TE and CM constraints. The latter is equivalent to setting $\rho = 1$ in $(\mathcal{P}_1)$ and $(\mathcal{P}_2)$, respectively. The resulting optimization problems are defined as

$$(\mathcal{P}_1') : \quad \min_{\mathbf{x}} f'(\mathbf{x})$$

$$s.t. \ \|\mathbf{x}\|_2^2 \leq P_{max},$$

and

$$(\mathcal{P}_2') : \quad \min_{\mathbf{x}} f'(\mathbf{x})$$

$$s.t. \ |x_n| = \sqrt{\frac{P_{max}}{TN}}, \ 1 \leq n \leq TN,$$

for the TE and CM constraints, respectively. Note, that $(\mathcal{P}_1')$ and $(\mathcal{P}_2')$ can be directly handled by Algorithm 1, though they can be solved via more efficient approaches since they are much simpler problems than $(\mathcal{P}_1)$ and $(\mathcal{P}_2)$. More specifically, $(\mathcal{P}_1')$ admits a solution given by,

$$\mathbf{x}^\star = (\tilde{\mathbf{H}}^H \tilde{\mathbf{H}} + \psi \mathbf{I}_T)^{-1} \tilde{\mathbf{H}}^H \mathbf{s}, \qquad (47)$$

where the Lagrange multiplier $\psi \in \mathbb{R}_+$ is set such that the TE constraint is met, e.g. by the application of a bisection method [43]. Problem $(\mathcal{P}_2')$ can be efficiently solved via the application of Algorithm 2 in [46].

In a similar manner for the radar part, the considered benchmarks are involving the SINR maximization of the radar-only system under the considered constraints. This is equivalent to setting $\rho = 0$ in optimization problems $(\mathcal{P}_1)$-$(\mathcal{P}_4)$, respectively. The resulting optimization problems are given by,

$$(\mathcal{P}_1'') : \quad \max_{\mathbf{x},\mathbf{w}} \gamma(\mathbf{x},\mathbf{w})$$

$$s.t. \ \|\mathbf{x}\|_2^2 \leq P_{max},$$

$$(\mathcal{P}_2'') : \quad \max_{\mathbf{x},\mathbf{w}} \gamma(\mathbf{x},\mathbf{w})$$

$$s.t. \ |x_n| = \sqrt{\frac{P_{max}}{TN}}, \ 1 \leq n \leq TN,$$

$$(\mathcal{P}_3') : \quad \min_{\mathbf{x},\mathbf{w}} \frac{1}{\gamma(\mathbf{x},\mathbf{w})} + \lambda \|\mathbf{x} - \mathbf{x}_0\|_2^2$$

$$s.t. \ \|\mathbf{x}\|_2^2 \leq P_{max},$$

and

$$(\mathcal{P}_4') : \quad \min_{\mathbf{x},\mathbf{w}} \frac{1}{\gamma(\mathbf{x},\mathbf{w})} + \lambda \|\mathbf{x} - \mathbf{x}_0\|_2^2$$

$$s.t. \ |x_n| = \sqrt{\frac{P_{max}}{TN}}, \ 1 \leq n \leq TN,$$

for the TE, CM, TE+SIM, and CM+SIM constraints, respectively. The proposed algorithmic solutions in the present paper can handle directly $(\mathcal{P}_1'')$, $(\mathcal{P}_2'')$, $(\mathcal{P}_3')$ and $(\mathcal{P}_4')$, as well. Furthermore, $(\mathcal{P}_1'')$ and $(\mathcal{P}_2'')$ have been extensively studied in the radar
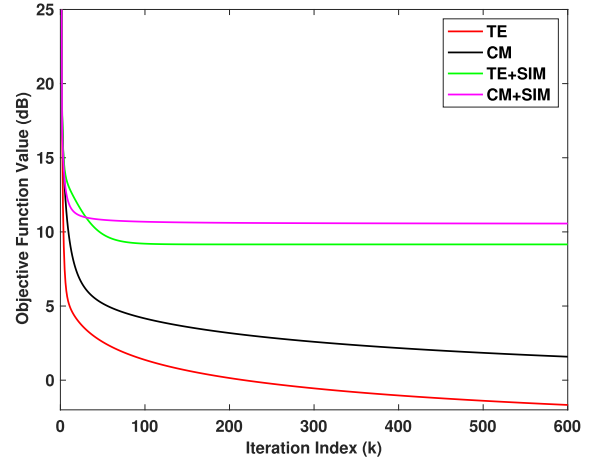

Fig. 3. Convergence study of the proposed algorithmic solutions for a DFRC system with $T = 16$ antennas at the transmitter serving $M = 4$ UTs. The trade-off and similarity parameters are set to $\rho = 0.5$ and $\lambda = 1$, respectively.

literature and thus, the approaches in [24], [26], [29], [38] can be also applied for deriving their solution.

B. Convergence Study

In Fig. 3, the convergence of the proposed algorithmic solutions is experimentally studied when the trade-off control parameter is set to $\rho = 0.5$. The average values of the objective functions per iteration for the different approaches are examined.

As it is observed, all of the considered approaches are rapidly converging to a stationary point. It is noteworthy to point out that the case of the TE constraint ("TE" curve) converges to a stationary point that corresponds to a lower objective value than the one of the CM constraint ("CM" curve). This is the case, since the feasible set of solutions is smaller for the CM case, than the TE one.

The former is a subset to the one defined for the case of the TE constraint. In other words, the performance of the CM case is lower bounded by that of the TE one. Similar conclusions can be reached when the similarity constraints are included in the previous two cases ("TE+SIM" and "CM+SIM," respectively). The similarity parameter is set to $\lambda = 1$. The case involving the TE constraint converges to a "better" optimal point compared to the one of the CM constraint for the common objective function in $(\mathcal{P}_3)$ and $(\mathcal{P}_4)$.

C. Bit Error Rate Performance of the Communication Part

We start with the evaluation of the performance of the communication part of the DFRC system. In Fig. 4, the average uncoded Bit Error Rate (BER) achieved by different techniques versus the transmit signal-to-noise ratio (SNR) is depicted. The trade-off parameter is set to $\rho = 0.9$. The transmit SNR is defined as $\mathbb{E}\{\|\mathbf{x}\|_2^2\}/\sigma_z^2$. In more detail, a DFRC system is considered for the cases of 1) TE ("TE-DFRC"), 2) CM ("CM-DFRC"), 3) TE+SIM ("TE+SIM-DFRC") and 4) CM+SIM ("CM+SIM-DFRC") constraints. The similarity parameter is set to $\lambda = 0.1$ in the corresponding cases. For comparison purposes, the cases of a
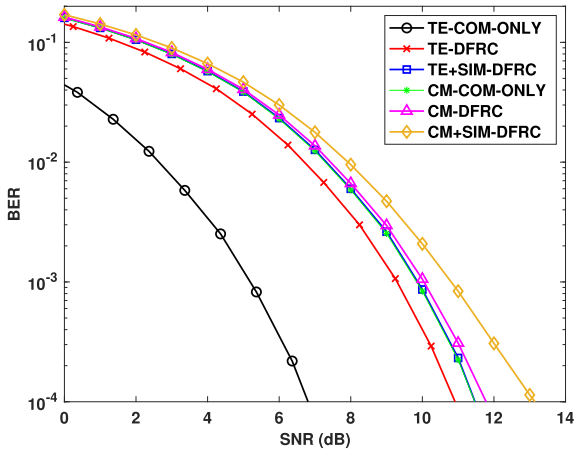
Fig. 4. BER versus transmit SNR curves of the DFRC system for the different techniques. The DFRC system has $T = 16$ transmit antennas and serves $M = 4$ UTs. The trade-off and similarity parameters are set to $\rho = 0.9$ and $\lambda = 0.1$, respectively.

TABLE I
RADAR RECEIVE SINR AND DETECTION PROBABILITY - TOTAL TRANSMISSION ENERGY CONSTRAINT

	SINR (dB)			Detection Probability (P_d)		
ρ	$\lambda = 0$	$\lambda = 0.1$	$\lambda = 1$	$\lambda = 0$	$\lambda = 0.1$	$\lambda = 1$
0.9	12.8165	12.7073	12.6528	0.5560	0.5498	0.5483
0.5	18.6851	15.5599	12.7345	0.9994	0.9610	0.5635
0.1	19.4547	15.7121	12.9373	1.0000	0.9692	0.6020
0	20.7078	16.2063	13.1010	1.0000	0.9882	0.6336

communication-only system under the TE ("TE-COM-ONLY") and the CM ("CM-COM-ONLY") constraints are considered, as well. The waveform design for these cases is based on the solutions of $(\mathcal{P}'_1)$ and $(\mathcal{P}'_2)$, respectively. As it was expected, the performance is worse for the approaches involving the similarity constraint ("TE+SIM-DFRC," "CM+SIM-DFRC") compared to the ones without it ("TE-DFRC," "CM-DFRC").

This is the case, since the similarity constraint enforces a specific structure to the transmission signals. In general, this structure does not promote the minimization of the MUI energy (2) which is related to the performance of the communication part, as discussed in Section III. Furthermore, the dual radar-communication function comes at a cost on the performance of the communication part, as it can be seen by comparing the curves of the DFRC systems to the communication-only counterparts. This impact on the performance is more severe for the TE constraint, as the "TE-DFRC" curve presents approximately 4 dB loss on the performance when compared to its communication-only counterpart ("TE-COM-ONLY"). On the other hand, for the CM constraint case, the DFRC system ("CM-DFRC") presents very small performance loss compared to its communication-only counterpart ("CM-COM-ONLY"). Note that in general, the systems under the TE constraint achieve better performance than the ones under the CM constraint for the reasons mentioned in the discussion of the convergence results in Fig. 3.

D. Total Transmission Energy Constraint

We now move to the evaluation of the performance of the DRFC system under the TE and the TE+SIM constraints. To that end, we plot the achievable sum-rate (5) of the two cases versus the transmit SNR in Figs. 5.(a)–(b). The performance of the communication-only system under the TE constraint is depicted in both figures for comparison purposes. In addition, for evaluating the performance of the radar part, as well, we present the radar receive SINR and the detection probability achieved by

the two cases in Table I. In the latter table, the performance of the corresponding radar-only systems is also shown for comparison purposes ($\rho = 0$). These cases involve the performance of the radar-only system under the TE and TE+SIM constraints. The joint waveform and filter design in the aforementioned cases is based on the solutions of $(\mathcal{P}''_1)$ and $(\mathcal{P}'_3)$, respectively, as described in Section V-A. The values of the trade-off parameter $\rho = \{0.1, 0.5, 0.9\}$ are considered for all the examined cases in Fig. 5 and the Table I. For the TE+SIM case, results are presented for two values of the similarity parameter, $\lambda = 0.1$ and $\lambda = 1$. The previous applies both on the results shown in Figs. 5.(a)-(b) and Table I, as well. The column for $\lambda = 0$ in Table I corresponds to the TE constraint case.

In Fig. 5.(a), the performance of the DFRC system for the TE constraint is depicted. As we can see, a decrease in the value of ρ has in general small impact on the performance of the communication system while adding more weight on the performance of the radar part. On the other hand, decreasing the ρ parameter's value from 0.9 to 0.5 results in a significant improvement on the radar receive SINR (Table I). As a consequence, the probability of detection is significantly improved, as well. Thus, it can be concluded that the DFRC system with the TE constraint has a communication part that appears to be robust to the changes of the trade-off parameter ρ. That is, the ρ parameter can be tuned easily to a value where both the radar and the communication parts can perform well and very close to the radar- and communication-only counterparts.

In Fig. 5.(b), the achievable sum-rate of a DFRC system under the TE+SIM constraint is presented. As can be seen, the similarity constraint has severe impact on the performance of the DFRC system due to the imposed strict structure on the transmitted waveforms. This was also discussed in the results of Fig. 4 in Section V-C. Thus, if high similarity is sought, significant degradation is observed on the achievable rate. This can be verified by checking the results for $\rho = 0.1$ and $\lambda = 1$ in Fig. 5.(b). Similar conclusions can be reached by inspecting Table I. High values of the λ parameter, impose high similarity to the reference waveform though this degrades the radar receive SINR and the detection probability, as well. Of course, by appropriately tuning the ρ and λ parameters, one may select the desired point of function based on the performances of the radar and the communication parts. Furthermore, the results in Table I verify the relation between the radar receive SINR and the detection probability. That is, the latter is a monotonically increasing function of the former.

For further insights on the radar part performance, the beam-pattern $P(\theta)$ is plotted for both the TE and TE+SIM cases in Figs. 6.(a)-(b). By denoting by $\mathbf{x}^\star$ and $\mathbf{w}^\star$, the optimal waveform
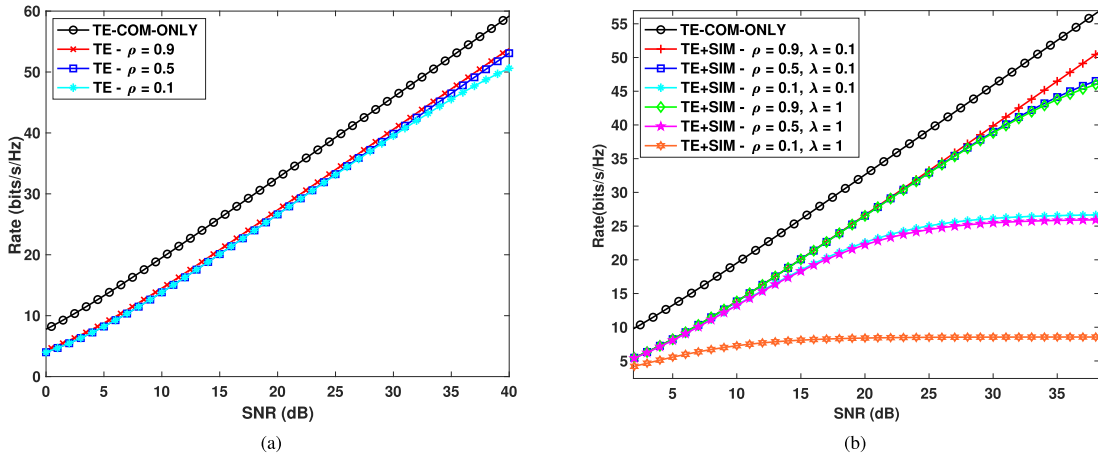
Fig. 5.   Achievable sum-rate versus transmit SNR for a DFRC system with $T = 16$ transmit antennas serving $M = 4$ users. (a) Total Transmission Energy Constraint, (b) Total Transmission Energy-plus-Similarity Constraint.

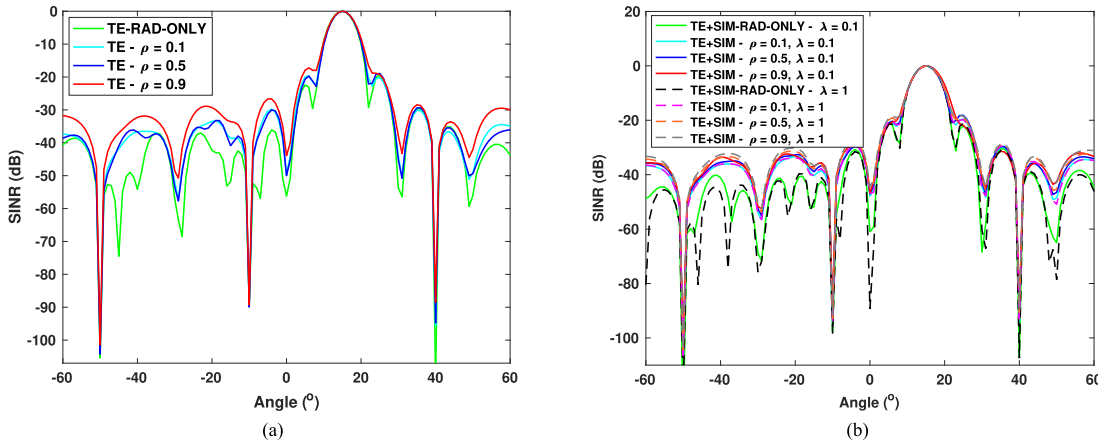Fig. 6.   Beampattern for a system with $T = 16$ transmit and $R = 8$ radar receive antennas. (a) Total Transmission Energy Constraint, (b) Total Transmission Energy-plus-Similarity Constraint.
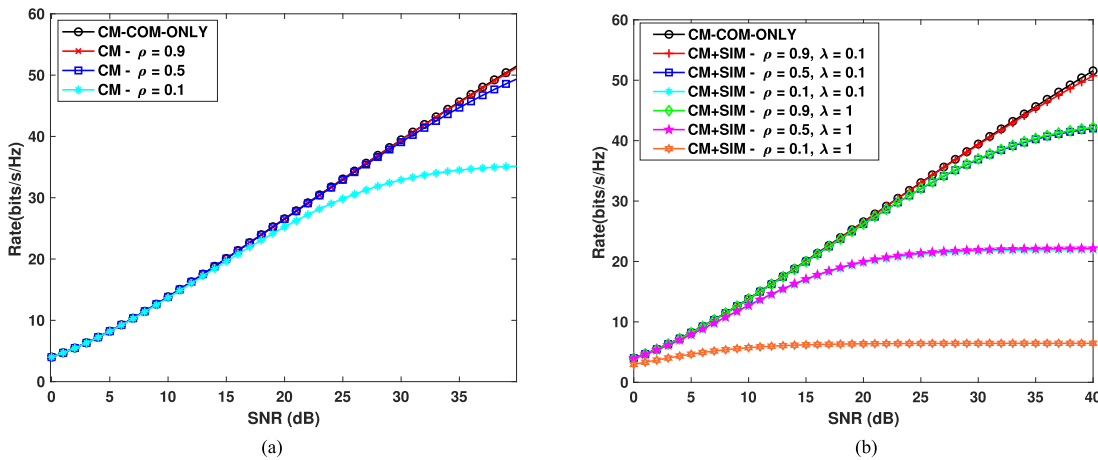

Fig. 7.   Achievable sum-rate versus transmit SNR for a DFRC system with $T = 16$ transmit antennas serving $M = 4$ users. (a) Constant-Modulus Constraint, (b) Constant-Modulus-plus-Similarity Constraint.
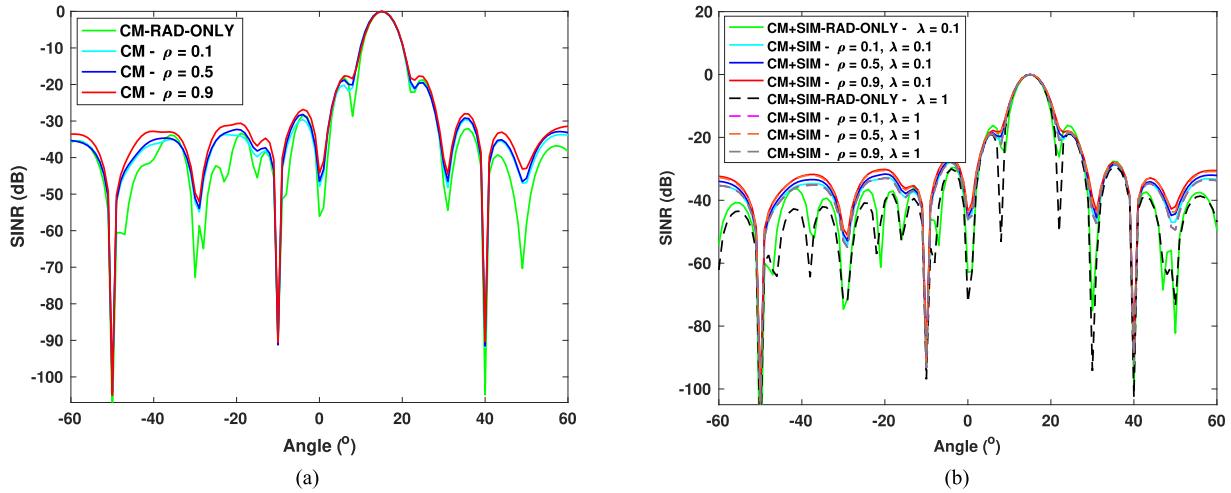
Fig. 8. Beampattern for a system with $T = 16$ transmit and $R = 8$ radar receive antennas. (a) Constant-Modulus Constraint, (b) Constant-Modulus-plus-Similarity Constraint.

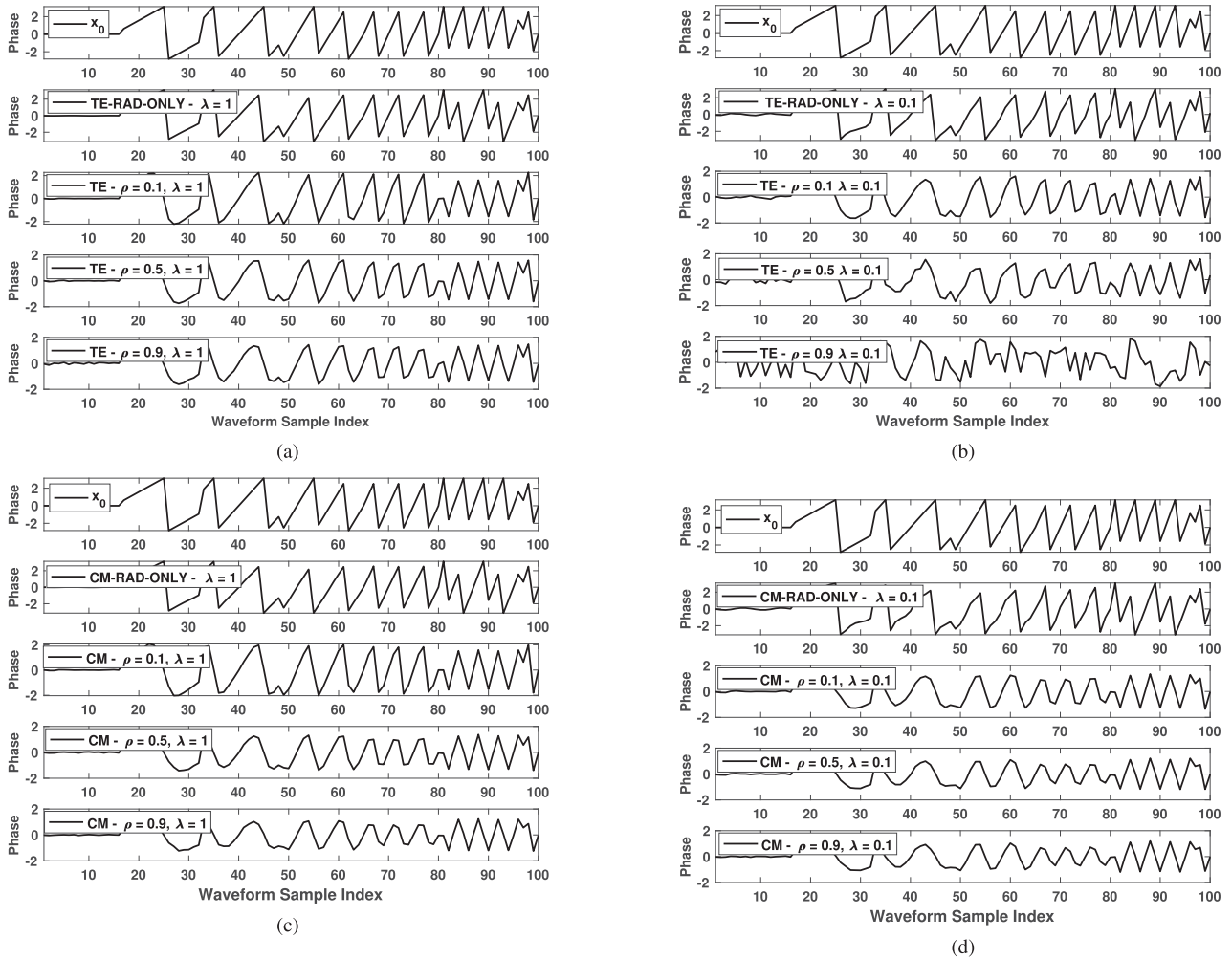Fig. 9. Phase of the derived waveforms for different values of the trade-off parameter ρ. A system with $T = 16$ transmit and $R = 8$ radar receive antennas is considered. (a) Total Transmission Energy Constraint, $\lambda = 1$, (b) Total Transmission Energy Constraint, $\lambda = 0.1$, (c) Constant-Modulus Constraint, $\lambda = 1$, (d) Constant-Modulus Constraint, $\lambda = 0.1$.

TABLE II
RADAR RECEIVE SINR AND DETECTION PROBABILITY - CONSTANT-MODULUS
CONSTRAINT

	SINR (dB)			Detection Probability (P_d)		
ρ	$\lambda = 0$	$\lambda = 0.1$	$\lambda = 1$	$\lambda = 0$	$\lambda = 0.1$	$\lambda = 1$
0.9	13.2781	12.8056	11.7744	0.6658	0.5768	0.3958
0.5	15.4549	14.1292	12.1195	0.9536	0.8125	0.4516
0.1	16.3068	14.6158	12.2007	0.9881	0.8798	0.4637
0	18.6748	15.1326	12.4960	1.0000	0.9002	0.4894

and radar receive filter, respectively, the beampattern is given by,

$$P(\theta) = |(\mathbf{w}^\star)^H \mathbf{A}(\theta)\mathbf{x}^\star|^2, \qquad (48)$$

where $\mathbf{A}(\theta)$ is defined in (11).

Both of the examined techniques are performing well, in a sense that they are placing relative deep nulls in the spatial directions of the interfering sources. Furthermore, the results are in line with the ones presented in Table I. The lower the ρ value is, the deepest is the null placed on an interfering source. As a consequence, the higher is the radar receive SINR/detection probability. Furthermore, high values for the similarity parameter λ result, in general, in less deep nulls on the interfering sources. This results in the degradation of the radar receive SINR/detection probability performance.

E. Constant-Modulus Constraint

We move now to the case of the DFRC system that functions under the CM and CM+SIM constraints. The achievable sum-rate is plotted for the latter cases versus the transmit SNR in Figs. 7.(a)–(b). In the same figures, the performance of the corresponding communication-only systems is shown. The radar receive SINR and the probability of target detection are presented in Table II. Following the presentation of the results in Table I, Table II includes also the SINR and the probability of detection achieved by the radar-only systems ($\rho = 0$). That is, problems $(\mathcal{P}_2'')$ and $(\mathcal{P}_4')$ are solved for the CM and CM+SIM constraints case, respectively. The values of the trade-off parameter are set again to $\rho = \{0.1, 0.5, 0.9\}$ for the results in Figs. 7.(a)–(b) and Table II. The similarity parameter is set again to $\lambda = 0.1$ and $\lambda = 1$ for the CM+SIM case. The column for $\lambda = 0$ in Table II corresponds to the CM constraint case.

The performance of the DFRC system under the CM constraint only is shown in Fig. 7.(a). For the cases of $\rho = 0.9$ and $\rho = 0.5$, the DFRC system achieves performance close to the one of the communication-only counterpart. For the case of $\rho = 0.1$, a significant degradation on the performance is presented for high SNR values. By inspecting the corresponding values in Table II, it can be seen that both the radar receive SINR and the detection probability are quite low for $\rho = 0.9$. Furthermore, they are improving significantly when decreasing the ρ parameter to the 0.5 value. Further gains can be seen on the SINR and the detection probability values when $\rho = 0.1$. Thus, it can be deduced that for the values of ρ that try to balance the performance of the communication and the radar parts, satisfactory performance may be achieved for both of them. If more weight is given to the communication side, the radar performance deteriorates and vice-versa.

In Fig. 7.(b), the achievable sum-rate of a DFRC system with the CM+SIM constrainted is presented. In a similar manner to the results in Fig. 5.(b), a high value for the similarity parameter results in degradation on achievable sum rate of the communication part. The results in Table II, show also a similar impact on the SINR and, as a consequence, to the probability of detection of the system. Again, it can be deduced that by appropriately tuning the ρ and λ parameters, one may achieve satisfactory performance for both the communication and the radar part of the DFRC system. It is noteworthy that the results in Table II, verify also the monotonically increasing relation between the radar receive SINR and the detection probability.

In Figs. 8.a-b, the beampattern $P(\theta)$ is plotted for both the CM and CM+SIM constraint case. Similar conclusions are drawn with the ones of Figs. 6.a-b. Furthermore, the results are in line with those reported in Table II.

F. Impact of the Similarity Constraint on the Transmit Waveform

As the final part of this section, the impact of the similarity constraint on the transmit waveform is examined. To do so, the angles of the transmit waveforms designed by the techniques involving the TE+SIM and CM+SM constraints are presented in Figs. 9.(a)-(b) and Figs. 9.(c)-(d) for $\lambda = 0.1$ and $\lambda = 1$, respectively. For comparison purposes the angles of the reference signal $\mathbf{x}_0$ are depicted on all these figures. The first 100 samples of each signal are shown for $\rho = \{0.1, 0.5, 0.9\}$. As expected, high λ values result in a better approximation of the $\mathbf{x}_0$ angles. On the contrary, small λ values result in a poorer approximation of the reference signal. Moreover, a decrease in the trade-off control parameter ρ, results in a better approximation of the $\mathbf{x}_0$ angles. This is the case since more weight is considered on the performance of the radar part over the communication one.

VI. CONCLUSION

In this paper, joint designs for the transmit waveform and the radar receive filter of DFRC systems are proposed. A multiple antenna BS serving multiple single antenna users on the downlink while aiming at the simultaneous detection of a radar target is assumed. The joint optimal designs for the transmit waveform and the radar receive filter are derived such that different spatial/temporal constraints are satisfied. Four multi-objective optimization problems are formulated aiming at jointly optimizing the MUI energy and radar receive SINR of the the communication and the radar part of the DFRC system, respectively. The problems are formulated based on the weighted sum method that combines the two objective functions into a composite one. The latter approach enables a flexible performance trade-off between the radar and the communication objectives. The resulting constrained optimization problems are difficult and nonconvex. The different cases of TE, CM and similarity to a known radar waveform constraints are considered. Efficient algorithmic solutions are developed based on the alternating optimization and GP frameworks. The convergence of the proposed solutions to a KKT-point of the respective problems is theoretically established. The performance of the

proposed methods is studied via numerical results where it is shown that one may achieve satisfactory performance for both the radar and communication parts, tailored for the needs of the considered application, by appropriately tuning the values of the corresponding parameters.

REFERENCES

[1] V. Cisco, "Cisco visual networking index: Forecast and trends, 2017-2022," *White Paper*, vol. 1, pp. 1–38, 2018.

[2] J. Lin, W. Yu, N. Zhang, X. Yang, H. Zhang, and W. Zhao, "A survey on internet of things: Architecture, enabling technologies, security and privacy, and applications," *IEEE Internet Things J.*, vol. 4, no. 5, pp. 1125–1142, Oct. 2017.

[3] A. Zanella, N. Bui, A. Castellani, L. Vangelista, and M. Zorzi, "Internet of Things for smart cities," *IEEE Internet Things J.*, vol. 1, no. 1, pp. 22–32, Feb. 2014.

[4] Federal Communications Commission (FCC), Connecting America: The national broadband plan, 2010. [Online]. Available: https://www.fcc.gov/general/national-broadband-plan

[5] Federal Communications Commission (FCC), FCC Proposes Innovative Small Cell Use in 3.5 GHz Band, 2012. [Online]. Available: https://www.fcc.gov/document/fcc-proposes-innovative-small-cell-use-35-ghz-band

[6] Defense Advanced Research Projects Agency (DARPA), Shared spectrum access for radar and communications (SSPARC), 2016. [Online]. Available: http://www.darpa.mil/program/sharedspectrum-access-for-radar-and-communications

[7] B. Paul, A. R. Chiriyath, and D. W. Bliss, "Survey of RF communications and sensing convergence research," *IEEE Access*, vol. 5, pp. 252–270, Dec. 2017.

[8] L. Zheng, M. Lops, Y. C. Eldar, and X. Wang, "Radar and communication coexistence: An overview: A review of recent methods," *IEEE Signal Process. Mag.*, vol. 36, no. 5, pp. 85–99, Sep. 2019.

[9] F. Liu, C. Masouros, A. P. Petropulu, H. Griffiths, and L. Hanzo, "Joint radar and communication design: Applications, state-of-the-art, and the road ahead," *IEEE Trans. Commun.*, vol. 68, no. 6, pp. 3834–3862, Jun. 2020.

[10] R. Saruthirathanaworakun, J. M. Peha, and L. M. Correia, "Opportunistic sharing between rotating radar and cellular," *IEEE J. Sel. Areas Commun.*, vol. 30, no. 10, pp. 1900–1910, Nov. 2012.

[11] J. A. Mahal, A. Khawar, A. Abdelhadi, and T. C. Clancy, "Spectral coexistence of MIMO radar and MIMO cellular system," *IEEE Trans. Aerosp. Electron. Syst.*, vol. 53, no. 2, pp. 655–668, Apr. 2017.

[12] B. Li, A. P. Petropulu, and W. Trappe, "Optimum co-design for spectrum sharing between matrix completion based MIMO radars and a MIMO communication system," *IEEE Trans. Signal Process.*, vol. 64, no. 17, pp. 4562–4575, Sep. 2016.

[13] B. Li and A. P. Petropulu, "Joint transmit designs for coexistence of MIMO wireless communications and sparse sensing radars in clutter," *IEEE Trans. Aerosp. Electron. Syst.*, vol. 53, no. 6, pp. 2846–2864, Dec. 2017.

[14] F. Liu, C. Masouros, A. Li, and T. Ratnarajah, "Robust MIMO beamforming for cellular and radar coexistence," *IEEE Wireless Commun. Lett.*, vol. 6, no. 3, pp. 374–377, Jun. 2017.

[15] F. Liu, C. Masouros, A. Li, T. Ratnarajah, and J. Zhou, "MIMO radar and cellular coexistence: A power-efficient approach enabled by interference exploitation," *IEEE Trans. Signal Process.*, vol. 66, no. 14, pp. 3681–3695, Jul. 2018.

[16] F. Liu, L. Zhou, C. Masouros, A. Li, W. Luo, and A. Petropulu, "Toward dual-functional radar-communication systems: Optimal waveform design," *IEEE Trans. Signal Process.*, vol. 66, no. 16, pp. 4264–4279, Aug. 2018.

[17] F. Liu, C. Masouros, A. Li, H. Sun, and L. Hanzo, "MU-MIMO communications with MIMO radar: From co-existence to joint transmission," *IEEE Trans. Wireless Commun.*, vol. 17, no. 4, pp. 2755–2770, Apr. 2018.

[18] X. Liu, T. Huang, N. Shlezinger, Y. Liu, J. Zhou, and Y. C. Eldar, "Joint transmit beamforming for multiuser MIMO communications and MIMO radar," *IEEE Trans. Signal Process.*, vol. 68, pp. 3929–3944, Aug. 2020.

[19] S. H. Dokhanchi, B. S. Mysore, K. V. Mishra, and B. Ottersten, "A mmWave automotive joint radar-communications system," *IEEE Trans. Aerosp. Electron. Syst.*, vol. 55, no. 3, pp. 1241–1260, Jun. 2019.

[20] Y. Wang, X. Wang, H. Liu, and Z. Luo, "On the design of constant modulus probing signals for MIMO radar," *IEEE Trans. Signal Process.*, vol. 60, no. 8, pp. 4432–4438, Aug. 2012.

[21] M. Soltanalian and P. Stoica, "Designing unimodular codes via quadratic optimization," *IEEE Trans. Signal Process.*, vol. 62, no. 5, pp. 1221–1234, Mar. 2014.

[22] J. Li, J. R. Guerci, and L. Xu, "Signal waveform's optimal-under-restriction design for active sensing," *IEEE Signal Process. Lett.*, vol. 13, no. 9, pp. 565–568, Sep. 2006.

[23] A. De Maio, S. De Nicola, Y. Huang, S. Zhang, and A. Farina, "Code design to optimize radar detection performance under accuracy and similarity constraints," *IEEE Trans. Signal Process.*, vol. 56, no. 11, pp. 5618–5629, Nov. 2008.

[24] C. Chen and P. P. Vaidyanathan, "MIMO radar waveform optimization with prior information of the extended target and clutter," *IEEE Trans. Signal Process.*, vol. 57, no. 9, pp. 3533–3544, Sep. 2009.

[25] M. M. Naghsh, M. Soltanalian, P. Stoica, M. Modarres-Hashemi, A. De Maio, and A. Aubry, "A doppler robust design of transmit sequence and receive filter in the presence of signal-dependent interference," *IEEE Trans. Signal Process.*, vol. 62, no. 4, pp. 772–785, Feb. 2014.

[26] G. Cui, H. Li, and M. Rangaswamy, "MIMO radar waveform design with constant modulus and similarity constraints," *IEEE Trans. Signal Process.*, vol. 62, no. 2, pp. 343–353, Jan. 2014.

[27] A. Aubry, A. De Maio, and M. M. Naghsh, "Optimizing radar waveform and Doppler filter bank via generalized fractional programming," *IEEE J. Sel. Topics Signal Process.*, vol. 9, no. 8, pp. 1387–1399, Dec. 2015.

[28] B. Tang and J. Tang, "Joint design of transmit waveforms and receive filters for MIMO radar space-time adaptive processing," *IEEE Trans. Signal Process.*, vol. 64, no. 18, pp. 4707–4722, Sep. 2016.

[29] L. Wu, P. Babu, and D. P. Palomar, "Transmit waveform/receive filter design for MIMO radar with multiple waveform constraints," *IEEE Trans. Signal Process.*, vol. 66, no. 6, pp. 1526–1540, Mar. 2018.

[30] S. K. Mohammed and E. G. Larsson, "Per-antenna constant envelope precoding for large multi-user MIMO systems," *IEEE Trans. Commun.*, vol. 61, no. 3, pp. 1059–1071, Mar. 2013.

[31] M. Biguesh and A. Gershman, "Training-based MIMO channel estimation: A study of estimator tradeoffs and optimal training signals," *IEEE Trans. Signal Process.*, vol. 54, no. 3, pp. 884–893, Mar. 2006.

[32] A. Sabharwal, P. Schniter, D. Guo, D. W. Bliss, S. Rangarajan, and R. Wichman, "In-band full-duplex wireless: Challenges and opportunities," *IEEE J. Sel. Areas Commun.*, vol. 32, no. 9, pp. 1637–1652, Sep. 2014.

[33] J. R. Guerci, "Cognitive radar: A knowledge-aided fully adaptive approach," in *Proc. IEEE Radar Conf.*, 2010, pp. 1365–1370.

[34] A. Aubry, A. DeMaio, A. Farina, and M. Wicks, "Knowledge-aided (potentially cognitive) transmit signal and receive filter design in signal-dependent clutter," *IEEE Trans. Aerosp. Electron. Syst.*, vol. 49, no. 1, pp. 93–117, Jan. 2013.

[35] G. Cui, X. Yu, V. Carotenuto, and L. Kong, "Space-time transmit code and receive filter design for colocated MIMO radar," *IEEE Trans. Signal Process.*, vol. 65, no. 5, pp. 1116–1129, Mar. 2017.

[36] E. Bjornson, E. A. Jorswieck, M. Debbah, and B. Ottersten, "Multiobjective signal processing optimization: The way to balance conflicting metrics in 5G systems," *IEEE Signal Process. Mag.*, vol. 31, no. 6, pp. 14–23, Nov. 2014.

[37] M. Alodeh *et al.*, "Symbol-level and multicast precoding for multiuser multiantenna downlink: A state-of-the-art, classification and challenges," *IEEE Commun. Surv. Tut.*, vol. 20, no. 3, pp. 1733–1757, Jul./Aug. 2018.

[38] B. Friedlander, "Waveform design for MIMO radars," *IEEE Trans. Aerosp. Electron. Syst.*, vol. 43, no. 3, pp. 1227–1238, Jul. 2007.

[39] T. Naghibi and F. Behnia, "MIMO radar waveform design in the presence of clutter," *IEEE Trans. Aerosp. Electron. Syst.*, vol. 47, no. 2, pp. 770–781, Apr. 2011.

[40] C. Rapp, "Effects of HPA-nonlinearity on a 4-DPSK/OFDM-signal for a digital sound broadcasting signal," *ESA Special Publication*, vol. 332, pp. 179–184, 1991.

[41] S. Haykin, *Communication Systems*. Hoboken, NJ, USA: John Wiley Sons, Inc., 2008.

[42] A. Farina and S. Pardini, "Track-while-scan algorithm in a clutter environment," *IEEE Trans. Aerosp. Electron. Syst.*, vol. AES-14, no. 5, pp. 769–779, Sep. 1978.

[43] D. P. Bertsekas, "Nonlinear programming," *J. Oper. Res. Soc.* vol. 48, no. 3, pp. 334–334, 1999.

[44] J. Tranter, N. D. Sidiropoulos, X. Fu, and A. Swami, "Fast unit-modulus least squares with applications in beamforming," *IEEE Trans. Signal Process.*, vol. 65, no. 11, pp. 2875–2887, Jun. 2017.

[45] M. A. Richards, *Fundamentals of Radar Signal Processing*. New York, NY, USA: McGraw-Hill Educ., 2014.

[46] S. Domouchtsidis, C. G. Tsinos, S. Chatzinotas, and B. Ottersten, "Symbol-level precoding for low complexity transmitter architectures in large-scale antenna array systems," *IEEE Trans. Wireless Commun.*, vol. 18, no. 2, pp. 852–863, Feb. 2019.

Christos G. Tsinos (Senior Member, IEEE) received the Diploma degree in computer engineering and informatics, the M.Sc. and Ph.D. degrees in signal processing and communication systems, and the M.Sc. degree in applied mathematics from the University of Patras, Greece, in 2006, 2008, 2013, and 2014, respectively.

From 2014 to 2020, he held a Postdoctoral Researcher, Research Associate and Research Scientist Positions with the University of Patras and with the University of Luxembourg, Luxembourg City, Luxembourg. He has recently been elected as an Assistant Professor with the University of Athens, Greece. He is also a Research Fellow with the SnT, University of Luxembourg. He was involved in a number of different Research and Development projects funded by national and/or EU funds. His current research interests include optimization and machine learning for signal processing and communications.

Aakash Arora (Student Member, IEEE) received the M.S. (Research) degree in electrical engineering from the Indian Institute of Technology Delhi, New Delhi, India, in 2017, and the Ph.D. degree in computer science from the Interdisciplinary Centre for Security, Reliability and Trust, University of Luxembourg, Luxembourg. He is currently holds a Research Associate position with the Interdisciplinary Centre for Security, Reliability and Trust, University of Luxembourg. His research interests include optimization algorithms, statistical signal processing, wireless communications, and machine learning.

Symeon Chatzinotas (Senior Member, IEEE) is currently a Full Professor / Chief Scientist I and the Head of the SIGCOM Research Group at SnT, University of Luxembourg, Luxembourg City, Luxembourg. He is coordinating the research activities on communications and networking, acting as a PI for more than 20 projects and main representative for 3GPP, ETSI, DVB. In the past, he was a Visiting Professor with the University of Parma, Italy, lecturing on 5G Wireless Networks. He has coauthored more than 450 technical papers in refereed international journals, conferences and scientific books. He was involved in numerous R&D projects for NCSR Demokritos, CERTH Hellas and CCSR, University of Surrey, Guildford, U.K. He was the co-recipient of the 2014 IEEE Distinguished Contributions to Satellite Communications Award and Best Paper Awards at EURASIP JWCN, CROWNCOM, ICSSC. He is currently in the Editorial Board of the IEEE TRANSACTIONS ON COMMUNICATIONS, IEEE OPEN JOURNAL OF VEHICULAR TECHNOLOGY, and the *International Journal of Satellite Communications and Networking*.

Björn Ottersten (Fellow, IEEE) received the M.S. degree in electrical engineering and applied physics from Linköping University, Linköping, Sweden, in 1986, and the Ph.D. degree in electrical engineering from Stanford University, Stanford, CA, USA, in 1990. He has held a research positions with the Department of Electrical Engineering, Linköping University, the Information Systems Laboratory, Stanford University, the Katholieke Universiteit Leuven, Leuven, Belgium, and the University of Luxembourg, Luxembourg. From 1996 to 1997, he was the Director of Research with ArrayComm, Inc., a start-up in San Jose, CA, USA, based on his patented technology. In 1991, he was appointed as a Professor of signal processing with the Royal Institute of Technology (KTH), Stockholm, Sweden. He is the Head of the Department for Signals, Sensors, and Systems, KTH, and the Dean of the School of Electrical Engineering, KTH. He is currently the Director of the Interdisciplinary Centre for Security, Reliability and Trust, University of Luxembourg. He was the recipient of the IEEE Signal Processing Society Technical Achievement Award, the EURASIP Group Technical Achievement Award, and the European Research Council advanced research grant twice. He has coauthored journal papers that were the recipient of the IEEE Signal Processing Society Best Paper Award in 1993, 2001, 2006, 2013, and 2019, and eight IEEE conference papers best paper awards. He is a Board Member of the IEEE Signal Processing Society, the Swedish Research Council and currently serves of the boards of EURASIP, and the Swedish Foundation for Strategic Research. Dr. Ottersten has served as the Editor-in-Chief of the *EURASIP Signal Processing*, and acted on the Editorial Boards of the IEEE TRANSACTIONS ON SIGNAL PROCESSING, IEEE SIGNAL PROCESSING MAGAZINE, IEEE OPEN JOURNAL FOR SIGNAL PROCESSING, *EURASIP Journal of Advances in Signal Processing,* and *Foundations and Trends in Signal Processing*. He is a Fellow of EURASIP.